High Level ab Initio Exploration on the Conversion of Carbon Dioxide into Oxazolidinones: The Mechanism and Regioselectivity

Wei-Hua Mu, Gregory A. Chasse, and De-Cai Fang*

College of Chemistry, Beijing Normal University, Beijing 100875, P.R. of China, and School of Chemistry, University of Wales, Bangor, Gwynedd, LL57 2UW, U.K.

Received: February 13, 2008; Revised Manuscript Received: April 29, 2008

Density functional theory (DFT) and second order Mϕller−Plesset perturbation (MP2) calculations, employing the 6-311++G(d,p) basis set, were carried out on alkyl-substituted aziridines to explore the reaction mechanisms and regioselectivity associated with their ring-opening conversions to oxazolidinones, in the presence of carbon dioxide. Computational results, employing the self-consistent reaction field polarizable continuum model (SCRF(PCM/Bader)), indicated that the conversions proceed with thermodynamic ease in THF solvent at room temperature. It is proposed that the *N*-alkylaziridine promotes ring opening through a S_N2 attack of the iodide ion, of catalytic lithium iodide, on the preformed complex. The oxazolidinone regioisomer ratio is highly sensitive to aziridine ring-carbon substitution. Therein, monophenyl substitutions show preference to opening more highly substituted carbon−nitrogen bonds, providing rationale as to why experimental works result in an exclusive oxazolidinone regioisomer product.

1. Introduction

Due to the excessive use and combustion of fossil fuels, the rate of production and release of carbon dioxide (CO_2) into the atmosphere has grown exponentially over the past century, with a variety of associated environmental problems. A great deal of work, in many differing fields, has been undertaken in the hopes of formulating effective means to reducing the percentage of CO_2 in the atmosphere. One method experimental chemists have identified is to efficiently convert CO_2 to other useful compounds. For example, Nguyen[1] and Pinhas[2] et al. have recently reported a facile method of converting CO_2 to oxazolidinones at room temperature. It has been established that selected chiral oxazolidinones may be used as antibacterial agents,[3] chiral synthons or auxiliaries;[4] they have also been widely used in the pharmaceutical industry.

As these methods make use of CO_2 as a starting material, mechanistic refinement and optimization thereof, would help promote widespread application and effect a subsequent reduction in atmospheric CO_2 deposition. It is therefore essential to have a quantitative understanding at the molecular level of the associated mechanisms for these processes.

Pinhas et al.[2] proposed a putative mechanism for these reactions (Figure 1), yet it had been subsequently established that **4a** is relatively unstable and may in fact reduce the likelihood of the **1a** → **4a** → **6a** pathway to zero.[5] Likewise, the alternate S_N2 pathway (**1a** → **5a** → **6a**) is also improbable, as QTAIM[6] topological analysis of **5a** (see the Supporting information), performed with the AIM2000 program,[7] indicated that there are two pairs of weak molecular interactions, mainly N3···C5 and C−H···O, with an interatomic distance of N3−C5 computed to be 2.906 Å (too long to be significant) at the SCRF(PCM/UA0)-B3LYP/6-311++G(d,p) level of theory, in tetrahydrofuran (THF) solvent. The relative energy of **5a** was also found to be only 0.03 kcal/mol more stable than the reactants. This is a value "on par" with the computational error attributed to DFT methods;[8] weak thermodynamic "incentive" for the reaction to proceed in this manner.

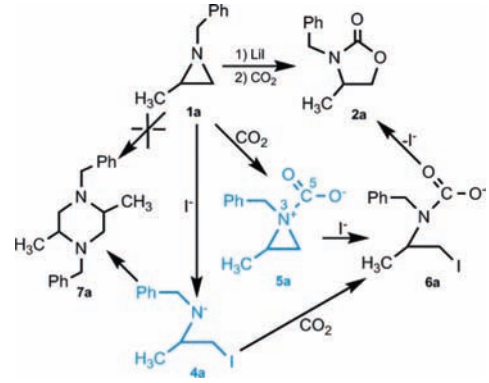

Figure 1. Diagrammatic representation of the putative reaction mechanism of the insertion of CO_2 into aziridine to form oxazolidinone, established by Pinhas et al.[2] One concerted (S_N1) and a pair of two-step (S_N2) mechanisms are shown on the right half of the figure. Structure **5a** shows the location of the N3 and C5 of interest.

SCHEME 1: General Reaction Studied in This Work

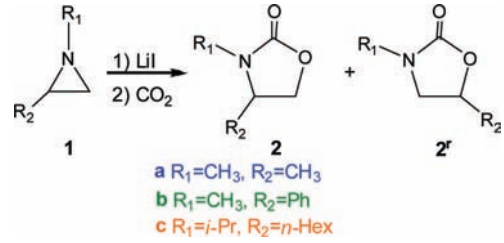

These results therefore discount two of three reaction pathways, indicating that insufficient information was derived in the empirical determinations to affirm which mechanistic process is operative. Likewise, an isolated theoretical study would not be sufficient to conclude which reaction path is most probably populated. It is therefore proposed to extend the

* To whom correspondence should be addressed.
† Beijing Normal University.
‡ University of Wales.

10.1021/jp801348w CCC: $40.75
Published on Web 07/01/2008

TABLE 1: Experimental Results on the Regioselectivity of Ring-Opening Reactions for Selected Aziridines

Entry	Main reactant	Time (h)	Product(s) and Ratio(%)		Overall Yield
	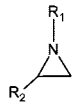		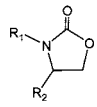	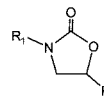	
	1		2	3	
25℃[a]	R_1=CH_2Ph, R_2=CH_3	4	61	39	83%
25℃[a]	R_1= pentyl, R_2= CH_3	4	66	34	86%
25℃[a]	R_1=CH_2Ph, R_2=CH_3		97	3	91%
25℃[b]	R_1= pentyl, R_2= CH_3		95	5	88%
25℃[b]	R_1= CH_2Ph, R_2=Ph	4		100	99%
100℃[c]	R_1=*i*-Pr, R_2=Ph	12	3	92	86%
100℃[c]	R_1=*i*-Pr, R_2=*n*-Hex	20	7	92	93%

[a] See ref 2b. [b] Products and yields for the reaction of **1** with LiI, hexamethylphosphoramide (HMPA) and CO_2. [c] See ref 1.

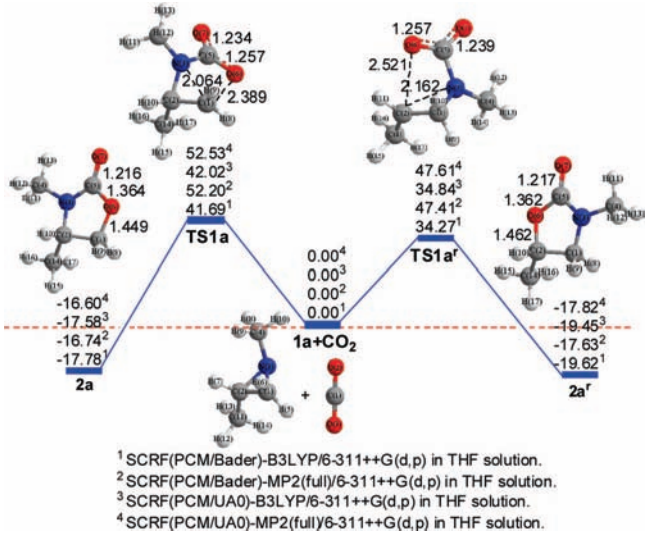

Figure 2. Reaction profile potential energy surface computed for the insertion of CO_2 into aziridine **1a** to form oxazolidinone, in the absence of catalyst. All structures were geometry-optimized and confirmed as residing at minima and first-order saddle points, computed at the SCRF-B3LYP/6-311++G(d,p) and SCRF-MP2(full)/6-311++G(d,p) levels of theory in THF, employing the PCM/UA0 or PCM/Bader model (energy in kcal/mol and bond length in Å).

theoretical work, with the experimental results as guide, to attain a full understanding of the reaction mechanisms at the molecular level.

The general reaction studied is shown in Scheme 1.

On the other hand, there is still no consensus on the underlying regioselectivity of the process. As shown in Table 1, experimental results of Pinhas et al.[2] show that the alkyl-substituted aziridines (with the exception of monophenyl C-substituted ones) prefer to ring-open through the less substituted carbon−nitrogen bond, and the results of Nguyen et al.[1] suggest that all alkyl-substituted aziridines prefer to ring-open via the more substituted carbon−nitrogen bond. An extensive work was therefore undertaken to identify and characterize the differing regioisomers produced from different alkyl-substituted aziridines. A quantitative understanding, at the molecular level, of these reaction types is sought from the theoretical exploration of the proposed mechanisms. Additionally, the debate may be pushed forward regarding the origins of, and resultant regioselectivity of, selected alkyl and phenyl C-substituted aziridines ring-openings in the presence of carbon dioxide. Herein, novel high-level computational results are presented, pioneering the theoretical characterization of highly effective chemical deposition of atmospheric CO_2.

2. Computational methods

The Becke-3−Lee−Yang−Parr (B3LYP)[10] and second-order Møller−Plesset perturbation (MP2)[11] methods were used for all calculations in this work, using the Gaussian 03 program package.[12] The default acceptance thresholds were employed for the geometry optimization of the most species involved in this paper, but some of them were optimized with tight convergence to get the correct curvature of the flat potential energy surface. The standard 6-311++G(d,p) Pople basis set[13] was used for C, H, O, N, Cl, Na and Li atoms. For the I atom, 1s, 1p and 1d diffusion functions were taken from the aug-cc-pVTZ-PP basis set,[14] and added to the standard 6-311G(d) basis set.[15] For convenience, a 6-311++G(d,p) notation is used from this point onward to denote the basis sets used.

To mimic experimental solvent conditions, the self-consistent reaction field (SCRF) polarizable continuum model (PCM)[16] was employed, with THF as solvent (dielectric constant ϵ = 7.58, 298.15 K). Previous work indicated that the default settings in the PCM/UA0 and PCM/UAHF models in the Gaussian 03 package underestimate the Van der Waals radius for Li atom, resulting in flawed characterization of Li-containing compounds. Our previous work[9] demonstrated that Bader's atomic radii[6b] are suitable to replace the original Van der Waals' radii for PCM calculation in GAUSSIAN program, which is denoted as the PCM/Bader model afterward. Therefore, only the PCM/Bader model was employed for the characterization of all Li-containing compounds within this work. Corresponding PCM/UA0 model calculations were carried out for compounds devoid of Li atoms for comparative analyses, as required.

The location of all structures on their associated potential energy hypersurfaces (PEHSs) were identified and characterized by the number of imaginary frequencies, at SCRF-B3LYP/6-311++G(d,p) or SCRF-MP2(full)/6-311++G(d,p) level of theory, employing the PCM/UA0 or PCM/Bader model. Intrinsic reaction coordinate (IRC)[17] computations were further used to trace some of the key reaction paths, to confirm that the TS structures obtained were in actuality adjacent to the minima proposed as lying on either side. The relative energies of all structures found at the MP2 level were corrected by their corresponding zero-point vibrational energies (ZPE), each scaled by a factor[18] of 0.9748, and the B3LYP ZPEs were scaled by a factor[19] of 0.9877.

3. Results and Discussion

3.1. Reaction Mechanism and Catalytic Role of LiI. As our previous results suggest, the alkyl substituents on the nitrogen atom have little effect on the overall reaction mechanism and insignificant perturbation of the energetic barrier for the ring-opening reaction of aziridine,[5] we simplified entry 7 of Table 1 to reactions **a** (Scheme 1), entries 1 to 4 to reaction **b**, whereas all groups in reaction **c** were retained as in the empirical determinations in the case **b2**. These modifications were made in service of a compromise between computational cost and retention of original reaction condition.

Model reactions **a**, **b**, **c** (as defined above) were used to theoretically characterize the conversion mechanism of CO_2 and aziridine to oxazolidinones, in both the absence and presence

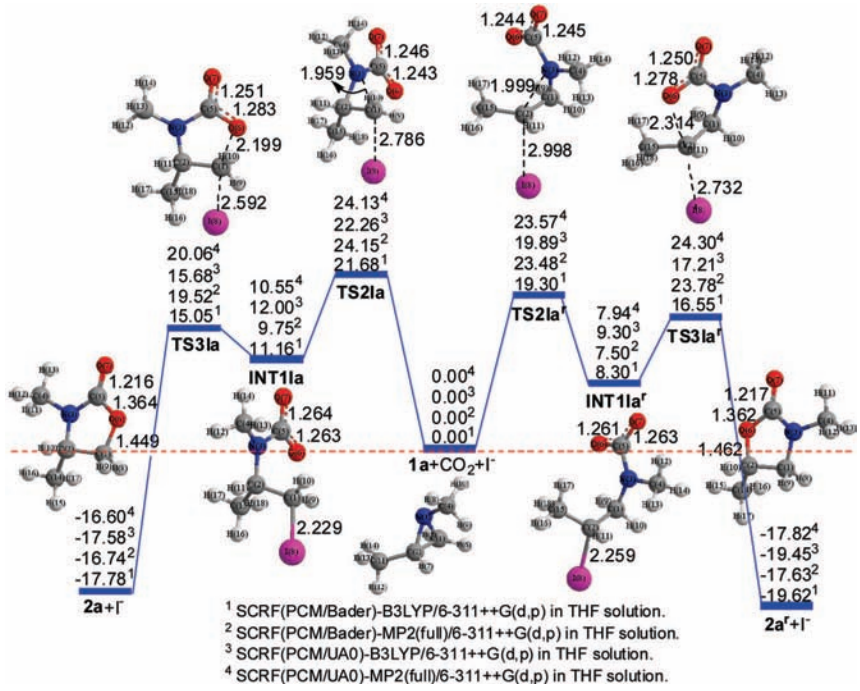

Figure 3. Reaction profile potential energy surface computed for the insertion of CO_2 into aziridine **1a** to form oxazolidinone, in the presence of catalytic I^-. All structures were geometry-optimized and confirmed as residing at minima and 1st order saddle-points, at the SCRF-B3LYP/6-311++G(d,p) and SCRF-MP2(full)/6-311++G(d,p) levels of theory in THF, employing the PCM/UA0 or PCM/Bader model (energy in kcal/mol and bond length in Å).

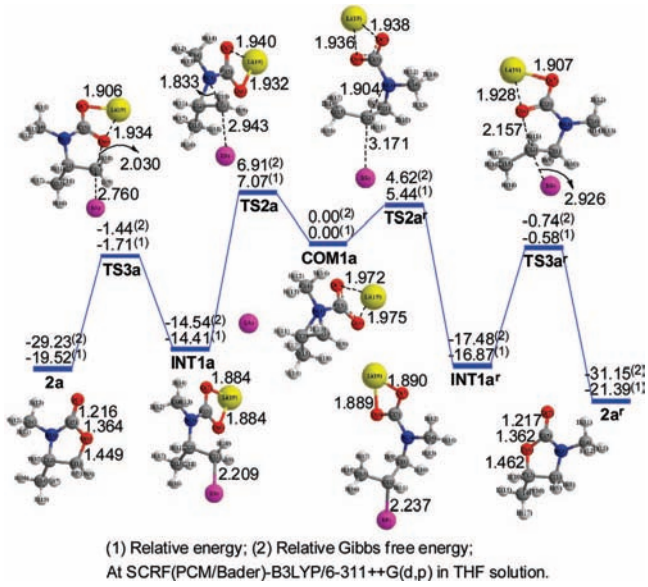

Figure 4. Reaction profile potential energy surface computed for the insertion of CO_2 into aziridine **1a** to form oxazolidinone, in the presence of catalytic LiI. All structures were geometry-optimized and confirmed as residing at minima and 1st order saddle-points, at the SCRF(PCM/Bader)-B3LYP/6-311++G(d,p) level of theory in THF (energy in kcal/mol and bond length in Å).

of catalytic LiI (Figures 2, 3, and 4, respectively), toward elucidating the role of LiI in the transformation of CO_2 into oxazolidinones.

The former (Figure 2) shows that the three-membered aziridine ring-opening (initiated by CO_2 attack) and subsequent five-membered ring formation, is a concerted (S_N1) process with just one transition state (**TS1a** or **TS1a^r**) located between the reactants and products. Two differing products may be obtained, **2a** and **2a^r**, where the latter appears to be more favorable, in direct opposition to the predictions of Pinhas et al.[2] The lower of the two activation barriers (via **TS1a^r**) is still relatively high (34.3 kcal/mol at SCRF(PCM/Bader)-B3LYP/6-311++G(d,p) level in THF) and highlights that it is improbable that either of the two reactions would proceed in the absence of catalytic LiI, under the given experimental conditions.[2a]

The mechanism was subsequently characterized in the presence of catalytic LiI. Because catalytic LiI exists as its ionic pair in THF, its contribution was assumed to be attributed to I^-, hence was modeled through the inclusion of one explicit iodide ion. As in the case of the uncatalyzed process, two competitive reaction pathways are observed (Figure 3) but differ from the former pair (Figure 2) in that an extra intermediate (**INT1Ia** or **INT1Ia^r**) is located between the reactants and the products. Although the uncatalyzed reactions are concerted, the I^--catalyzed reactions proceed in a bimolecular (S_N2) manner.

The corresponding ring-opening energy barriers are lowered from 41.69 and 34.27 kcal/mol to 21.68 and 19.30 kcal/mol, respectively, at the SCRF(PCM/Bader)-B3LYP/6-311++G(d,p) level of theory, in THF solvent. The Cartesian components of the force vectors ascribed to the atoms associated with the first vibrational modes of **TS2Ia** and **TS2Ia^r** ($-424i$ cm^{-1} and $-336i$ cm^{-1}, respectively) at the same level of theory indicated that the three-membered aziridine ring is opened by the synchronous attack of CO_2 and I^-, to form **INT1Ia** and **INT1Ia^r**, respectively. This is followed by the approach of O6 to C2, through which **INT1Ia^r** is converted to the more stable **2a^r**. These results also show that the preferred product is **2a^r** rather than **2a**, again in opposition to which has been previously reported.[2]

Comparison of the geometric structures optimized at differing levels of theories shows that the maximal variance in the bond lengths is less than 0.05 Å for most of the stationary points (Table 2). However, for C−I bonds in **TS2Ia** and **TS2Ia^r**, the maximal variance in the bond lengths is ~0.16−0.29 Å, which prompted us to compare the corresponding energy difference further. The results show a relative energy difference no bigger than 1.5 kcal/mol (Table 3), within the computational error

TABLE 2: Comparison of Selected Bond Lengths (in Å) in Some Geometric Structures Optimized at the SCRF(PCM/Bader)-B3LYP/6-311++G(d,p) (B3/Bader), SCRF(PCM/UA0)-B3LYP/6-311++G(d,p) (B3/PCM), SCRF(PCM/Bader)-MP2(full)/6-311++G(d,p) (MP2/Bader) and SCRF (PCM/UA0)-MP2(full)/6-311++G(d,p) (MP2/PCM) levels in THF Solution

	TS2Ia				**TS2Ia^r**			
	C(1)−N(3)	C(5)−O(6)	C(5)−O(7)	C(1)−I(8)	C(2)−N(3)	C(5)−O(6)	C(5)−O(7)	C(2)−I(8)
B3/Bader	1.959	1.243	1.246	2.786	1.999	1.244	1.245	2.998
B3/PCM	1.958	1.243	1.245	2.782	2.000	1.244	1.244	2.993
MP2/Bader	1.943	1.246	1.249	2.618	1.974	1.247	1.249	2.709
MP2/PCM	1.945	1.246	1.248	2.615	1.977	1.247	1.248	2.706
	INT1Ia				**INT1Ia^r**			
	C(1)−N(3)	C(5)−O(6)	C(5)−O(7)	C(1)−I(8)	C(2)−N(3)	C(5)−O(6)	C(5)−O(7)	C(2)−I(8)
B3/Bader	2.442	1.263	1.264	2.229	2.458	1.261	1.263	2.259
B3/PCM	2.439	1.263	1.263	2.230	2.456	1.261	1.262	2.257
MP2/Bader	2.444	1.264	1.264	2.181	2.429	1.262	1.264	2.194
MP2/PCM	2.450	1.263	1.262	2.180	2.429	1.262	1.263	2.194
	TS3Ia				**TS3Ia^r**			
	C(1)−O(6)	C(5)−O(6)	C(5)−O(7)	C(1)−I(8)	C(2)−O(6)	C(5)−O(6)	C(5)−O(7)	C(2)−I(8)
B3/Bader	2.199	1.283	1.251	2.592	2.314	1.278	1.250	2.732
B3/PCM	2.205	1.282	1.250	2.586	2.321	1.277	1.250	2.718
MP2/Bader	2.077	1.287	1.248	2.561	2.147	1.285	1.247	2.664
MP2/PCM	2.080	1.287	1.247	2.557	2.149	1.284	1.246	2.659
	2a				**2a^r**			
	C(1)−O(6)	C(5)−O(6)	C(5)−O(7)		C(2)−O(6)	C(5)−O(6)	C(5)−O(7)	
B3/Bader	1.449	1.364	1.216		1.462	1.362	1.217	
B3/PCM	1.448	1.365	1.215		1.462	1.363	1.216	
MP2/Bader	1.442	1.365	1.216		1.452	1.363	1.216	
MP2/PCM	1.442	1.365	1.216		1.452	1.364	1.216	

TABLE 3: Total and Relative Energies for Selected Geometric Structures, Optimized at SCRF(PCM/Bader)-MP2(full)/6-311++G(d,p) (MP2) and SCRF(PCM/Bader)-MP2(full)//B3LYP/6-311++G(d,p) (MP2//B3LYP) Levels in THF Solution

		TS2Ia	**INT1Ia**	**TS3Ia**	**TS2Ia^r**
total energy (au)	MP2	−7317.977501	−7318.001546	−7317.985873	−7317.978760
	MP2//B3LYP	−7317.976128	−7317.999783	−7317.983853	−7317.976906
relative energy (kcal/mol)	−0.86	−1.11	−1.27	−1.16	
		INT1Ia^r	**TS3Ia^r**	**2a**	**2a^r**
total energy (au)	MP2	−7318.005514	−7317.978847	−400.344160	−400.345480
	MP2//B3LYP	−7318.003712	−7317.976606	−400.3434611	−400.3447191
relative energy (kcal/mol)	−1.13	−1.41	−0.44	−0.48	

attributed to DFT methods.[8] Taking a look at Figure 2 and 3, one can see that the potential energy surfaces indicate a uniform trend in the preference of the predominant product, no matter whether the B3LYP or MP2(full) method is used, employing the PCM/Bader or PCM/UA0 SCRF model. In summary, the four sets of results show no difference in oxazolidinone regioisomers product ratio prediction; therefore, only results obtained at the SCRF(PCM/Bader)-B3LYP/6-311++G(d,p) level of theory are shown in the following figures.

Although the 19.30 kcal/mol energetic barrier for the insertion of CO_2 into the aziridine ring for the I^--catalyzed process (Figure 3) is much lower than that of the uncatalyzed process (Figure 2), it was of a magnitude requiring further theoretical investigation to identify other more energetically probable reaction pathways. Preliminary exploratory computations showed that the reaction could be further facilitated if Li^+ was also included in the models. Due to the aforementioned limitations of the default PCM/UA0 model in characterizing Li-containing compounds,[9] only PCM/Bader model results are presented from this point onward.

The (I^-/Li^+)-catalyzed reaction mechanism (Figure 4) is nearly identical to that of the I^--catalyzed one (Figure 3). When CO_2 is bubbled into the reaction solution,[2] the ionic pair of I^- and Li^+ will separate and react with **1a** and CO_2 to form **COM1a** prior to the ring-opening. Due to the formation of **COM1a**, the energetic barriers for the ring-opening step are brought down to 7.07 and 5.44 kcal/mol, respectively, much lower than those of the corresponding subsequent ring-closure steps. The latter (ring-closure) therefore becomes the rate-determining step (RDS) in the (I^-/Li^+)-catalyzed case, in direct contrast to the ring-opening RDS of the I^--catalyzed reaction (Figure 3). The energetic ring-closure barrier for the formation of **2a** is 12.70 kcal/mol (vs 16.29 kcal/mol for **2a^r**), signaling that the reaction proceeds with relative ease to **2a** in THF at room temperature, in agreement with the main product observed in experiment.[2] It is therefore essential that both I^- and Li^+ are included in models for this reaction. Overall, this reaction is exothermic and ∼20 kcal/mol is released in the formation of the final product **2a**.

Considering that the lithium cation may complex with THF molecule in the solution, we have further tried a case including one molecule of THF in the reaction, based on the I^-/Li^+-catalyzed one (Figures S5 and S6 in the Supporting Information). The corresponding reaction mechanism (Figure

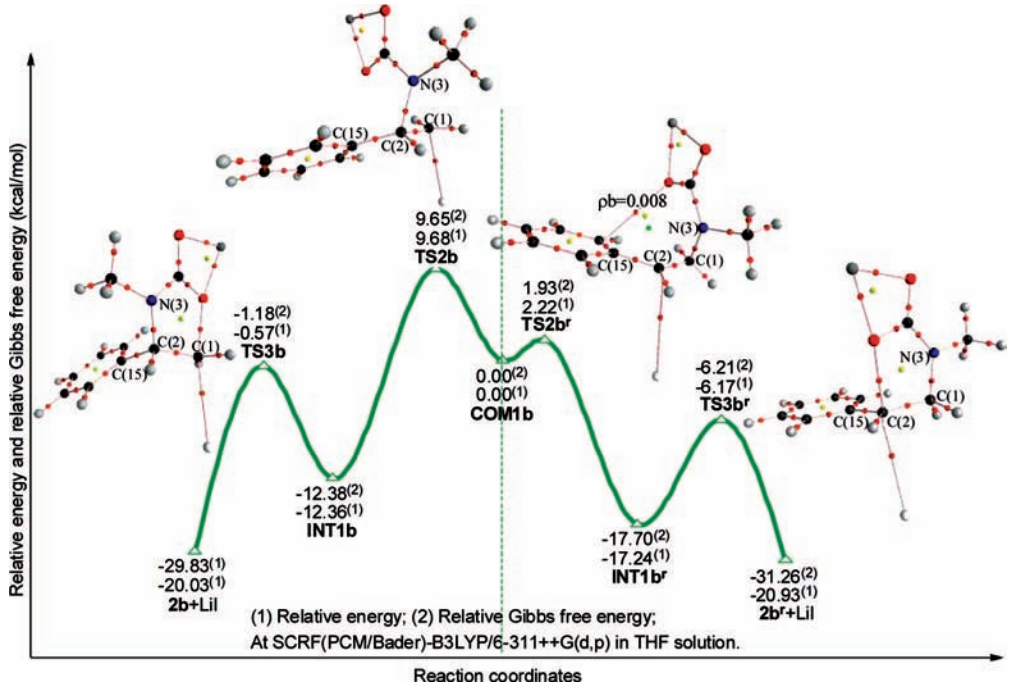

Figure 5. Reaction profile potential energy surface computed for the insertion of CO_2 into aziridine **1b** to form oxazolidinone, in the presence of catalytic LiI. All structures were geometry-optimized and confirmed as residing at minima and 1st order saddle-points, at the SCRF(PCM/Bader)-B3LYP/6-311++G(d,p) level of theory in THF (energy in kcal/mol and bond length in Å).

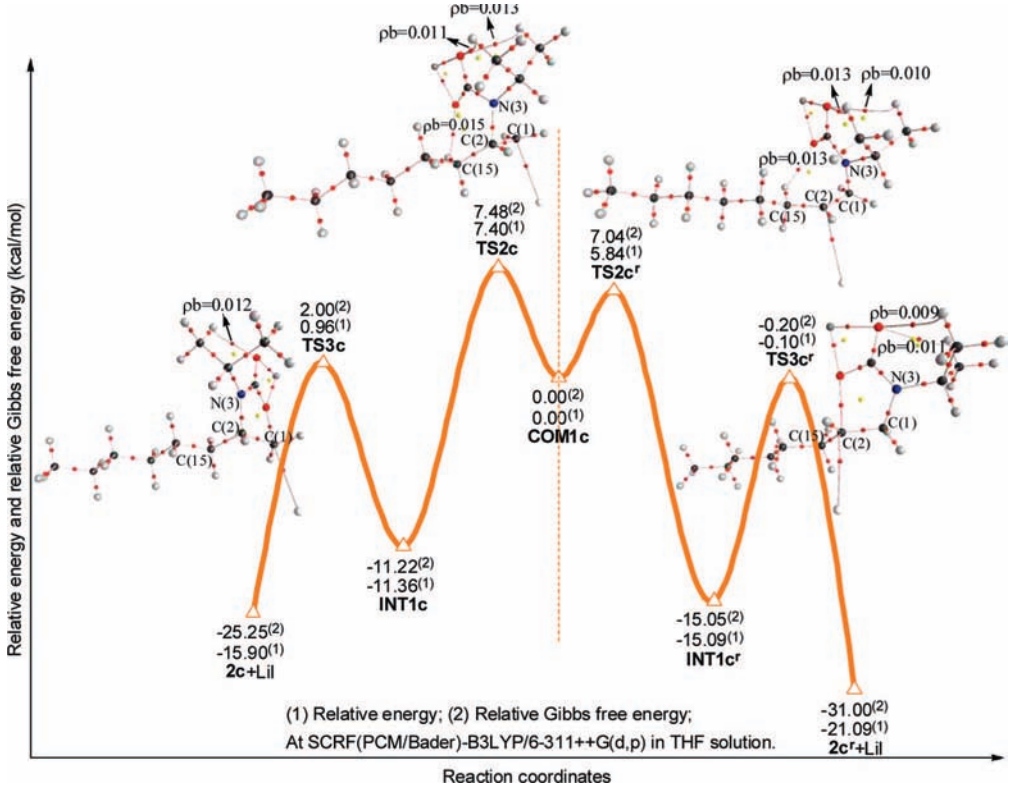

Figure 6. Reaction profile potential energy surface computed for the insertion of CO_2 into aziridine **1c** to form oxazolidinone, in the presence of catalytic LiI. All structures were geometry-optimized and confirmed as residing at minima and 1st order saddle-points, at the SCRF(PCM/Bader)-B3LYP/6-311++G(d,p) level of theory in THF (energy in kcal/mol, electron density in Au and bond length in Å).

S6 in the Supporting Information) and potential energy surface are almost the same as shown in Figure 4, which means that the THF molecule does not affect much on the reaction mechanism and the prediction of the predominant product, thus the implicit PCM model is proper in the description of the solvent effect here.

TABLE 4: Selected Bond Lengths (Å) Relative to C(1) and C(2) in Selected Numbering Stationary Points of Reactions b and c

stationary points	TS2b	TS3b	TS2b^r	TS3b^r	TS2c	TS3c	TS2c^r	TS3c^r
$R_{C(1)-C(2)}$	1.46	1.52	1.46	1.52	1.46	1.52	1.46	1.51
$R_{C(2)-C(15)}$	1.50	1.52	**1.45**	**1.44**	1.52	1.54	**1.49**	**1.49**

3.2. Regioselectivity of the Ring-Opening Reaction of Aziridine 1. The potential energy surfaces and topological graphs for selected stationary points in reactions **b** and **c** are shown in Figures 5 and 6, respectively. Due to the help of the phenyl ring, when the aziridine ring in **1b** breaks between C(2) and N(3), the electrons on C(2) in **TS2b^r** and **TS3b^r** are more delocalized than those on C(1) in **TS2b** and **TS3b**. This is manifested in the shortened C(2)−C(15) bond length in the stationary points (∼1.44−1.45 Å) of the former, relative to those in the latter (∼1.50−1.52 Å) (Table 4). Additionally, there is a weak C−H···O hydrogen bond interaction between one of the phenyl hydrogen atoms and one of the carbon dioxide oxygen atoms in **TS2b^r** (ρb = 0.008, Figure 5), whereas no similar interaction could be observed in the AIM topological graph of **TS2b**. Thus, both the ring-opening and ring-closing energy barriers on the pathway to **2b^r** are much lower than those leading to **2b.** That is, the energetic barriers corresponding to **TS2b^r** and **TS3b^r** are much lower than those corresponding to **TS2b** and **TS3b**, with **2b^r** the sole resultant regioisomer product.

For reaction **c** (Figure 6), similar weak C−H···O hydrogen bond interactions are observed between one of oxygen atoms in carbon dioxide and one of hydrogen atoms in the *n*-Hex or isopropyl (with $\rho b \approx 0.009-0.013$), observed not only in **TS2c^r** and **TS3c^r** but also in **TS2c** and **TS3c**. Additionally, with the phenyl group on C(2) in **1b** replaced by an *n*-Hex group in **1c**, the weakening of electron delocalization on C(2) is observed in **TS2c^r** and **TS3c^r**. As shown in Table 4, the bond lengths of C(2)−C(15) in **TS2c^r** and **TS3c^r** (1.49 Å) are only ∼0.03−0.05 Å shorter than the corresponding ones in **TS2c** and **TS3c** (1.52−1.54 Å), in contrast to corresponding ∼0.05−0.08 Å reductions from **TS2b** to **TS2b^r**, or **TS3b** to **TS3b^r**. Both aspects mentioned above lead to a smaller relative energetic difference between **TS2c^r** and **TS2c** (1.56 kcal/mol vs 7.46 kcal/mol between **TS2b^r** and **TS2b**), or between **TS3c^r** and **TS3c**(1.06 kcal/mol, vs 5.60 kcal/mol between **TS3b^r** and **TS3b**). Thus, two regioisomers (**2c^r** and **2c**) could be obtained, with the more thermodynamically stable product **2c^r** as the predominant regioisomer, in accordance with Nguyen et al.'s[1] experimental reports.

As a whole, when the alkyl substitutent on one of the aziridine ring carbons is a methyl group (reaction **a**), aziridine **1a** prefers to ring-open through the less substituted carbon−nitrogen bond, with **2a** as the major resultant product. However, when the alkyl substitutent on one of the aziridine ring carbons is changed to a phenyl group (reaction **b**), aziridine **1b** prefers to ring-open through the more highly substituted carbon−nitrogen bond, with **2b^r** the sole resultant product. When the alkyl substitutent on one of the aziridine ring carbons is changed to *n*-Hex (reaction **c**) and the nitrogen is isopropyl-substituted, aziridine **1c** also prefers to ring-open through the more substituted carbon−nitrogen bond, with **2c^r** as the major resultant product and showing larger **2c^r/2c** ratio (92:7) than for **2a^r/2a** (2:3).

Our exploratory computational results are in agreement with corresponding empirical data in terms of predicting product distributions, with the in silico characterizations offering more detailed mechanistic information at molecular level. The highest energy barrier leading to the major product in these reactions is within ∼15.0 kcal/mol, suggesting that these reactions may proceed with relative ease at room temperature, with no need to reflux prior to adding bubbled carbon dioxide at the outset of the reaction. This is a promising and potentially significant finding, which may perhaps lead to the simplification of the corresponding experimental conditions and associated steps therein.

4. Conclusions

High level density functional theory (DFT) and second order Møller−Plesset perturbation theory (MP2) computations, employing PCM/UA0 and PCM/Bader models, have been carried out to characterize the insertion of CO_2 into aziridine to form oxazolidinone, in the presence of catalytic LiI. Results revealed that the presence of both I^- and Li^+ are essential for accurate modeling of this reaction. The inclusion of iodide anion decreases the energy barrier of the rate-determining step (RDS) from 34.27 to 19.30 kcal/mol. The inclusion of lithium cation in the models makes the reaction more exothermic and lowers the RDS energetic barriers to within 15.0 kcal/mol. This suggests a potential and significant simplification of the corresponding experimental conditions and associated steps therein.

Computational characterization of the insertion mechanism, and its associated regioselectivity, suggests that a complex composed of one molecule each of aziridine and carbon dioxide, together with Li^+ and I^-, is formed prior to the opening of the aziridine three-membered ring. Alkyl substitution on an aziridine ring carbon significantly affects the ring-opened product ratio, wherein an aziridine phenyl-substituted at a single carbon leads to single product, formed through the breaking of the more highly substituted aziridine carbon−nitrogen bond. This is in contrast to the differentially substituted aziridines, which lead to the production of two regioisomers, whose product ratio is altered by aziridine ring-carbon substituent identity.

Acknowledgment. This work was supported by the National Nature Science Foundation of China (20773016), the Program for New Century Excellent Talents in University (NCET-04-0146), the Major State Basic Research Development Program (2004CB719900) and High-powered Computing Center of Beijing Normal University for partial CPU times. G.A.C. is thankful to CAFMaD (Wales, U.K.) for support. G.A.C. and D.C.F. thank GIOCOMMS for supporting regular academic exchanges and opportunities for young scholars, making this and other related works truly international in nature.

Supporting Information Available: Complete ref 12. Energies, frequencies, Carteisan coordinates, and figures of topological graphics, numbering systems, and stationary points of compounds are given in Figures S1−S8 and Tables S1−S24. This material is available free of charge via the Internet at http://pubs.acs.org.

References and Notes

(1) Miller, A. W.; Nguyen, S. T. *Org. Lett.* **2004**, *6*, 2301.

(2) (a) Hancock, M. T.; Pinhas, A. R. *Tetrahedron Lett.* **2003**, *44*, 5457. (b) Hancock, M. T.; Pinhas, A. R. *Synthesis* **2004**, *14*, 2347.

(3) (a) Weidner-Wells, M. A.; Boggs, C. M.; Foleno, B. D.; Wira, E.; Bush, K.; Goldschmidt, R. M.; Hlasta, D. J. *Bioorg. Med. Chem. Lett.* **2001**, *11*, 1829. (b) Ciske, F. L.; Barbachyn, M. R.; Genin, M. J.; Grega, K. C.; Lee, C. S.; Dolak, L. A.; Seest, E. P.; Watt, W.; Adams, W. J.; Friis, J. M.; Ford, C. W.; Zurenko, G. E. *Bioorg. Med. Chem. Lett.* **2003**, *13*, 4235. (c) Cui, Y.; Dang, Y.; Yang, Y.; Zhang, S.; Ji, R. *Eur. J. Med. Chem.* **2005**, *40*, 209. (d) Wang, G.; Ella-Menye, J.-R.; Sharma, V. *Bioorg. Med. Chem. Lett.* **2006**, *16*, 2177.

(4) (a) Nakamura, T.; Hashimoto, N.; Ishizuka, T.; Kunieda, T. *Tetrahedron Lett.* **1997**, *38*, 559. (b) Gibson, C. L.; Gillon, K.; Cook, S. *Tetrahedron Lett.* **1998**, *39*, 6733. (c) Adam, W.; Bosio, S. G.; Turro, N. J. *J. Am. Chem. Soc.* **2002**, *124*, 8814. (d) Hein, J. E.; Hultin, P. G. *Tetrahedron: Asym.* **2005**, *16*, 2341. (e) Li, J.-F.; Yang, R.; Nie, L.; Yang, L.-J.; Huang, R.; Lin, J. *J. Peptide Res.* **2005**, *66*, 319. (f) Kotake, T.; Hayashi, Y.; Rajesh, S.; Mukai, Y.; Takiguchi, Y.; Kimura, T.; Kiso, Y. *Tetrahedron* **2005**, *61*, 3819.

(5) Mu, W.-H.; Wang, C.; Fang, D.-C. *J. Mol. Struct. (THEOCHEM)* **2007**, *806*, 171.

(6) (a) Bader, R. F. W. *Chem. Rev.* **1991**, *91*, 893. (b) Bader, R. F. W. *Atoms in Molecules: a Quatum Theory*; Clarendon Press: Oxford, U.K., 1990.

(7) (a) Biegler-Konig, F.; Schonbohm, J.; Bayles, D. *J. Comput. Chem.* **2001**, *22*, 545. (b) Biegler-Konig, F.; Schonbohm, J. *J. Comput. Chem.* **2002**, *23*, 1489.

(8) Young D. C. *Computational Chemistry: A Practical Guide for Applying Techniques to Real World Problems*: John Wiley & Sons, Inc.: New York, 2001.

(9) Mu, W.-H.; Chasse, G. A.; Fang, D.-C. *Int. J. Quantum Chem.* **2008**, *108*, 1422.

(10) (a) Becke, A. D. *J. Chem. Phys.* **1993**, *98*, 5648. (b) Lee, C.; Yang, W.; Parr, R. G. *Phys. Rev. B* **1988**, *37*, 785.

(11) Mϕller, C.; Plesset, M. S. *Phys. Rev.* **1934**, *46*, 618.

(12) Frisch, M. J. et al. *Gaussian 03*, revision B.02; Gaussian, Inc.: Pittsburgh, PA, 2003.

(13) (a) Krishnan, R.; Binkley, J. S.; Seeger, R.; Pople, J. A. *J. Chem. Phys.* **1980**, *72*, 650. (b) Clark, T.; Chandrasekhar, J.; Spitznagel, G. W.; Schleyer, P. v. R. *J. Comput. Chem.* **1983**, *4*, 294.

(14) (a) Peterson, K. A.; Figgen, D.; Goll, E.; Stoll, H.; Dolg, M. *J. Chem. Phys.* **2003**, *119*, 11113. (b) Peterson, K. A. *J. Chem. Phys.* **2003**, *119*, 11099.

(15) Glukhovtsev, M. N.; Pross, A.; McGrath, M. P.; Radem, L. *J. Chem. Phys.* **1995**, *103*, 1878.

(16) (a) See examples Miertus, S.; Scrocco, E.; Tomasi, J. *Chem. Phys.* **1981**, *55*, 117. (b) Miertus, S.; Tomasi, J. *Chem. Phys.* **1982**, *65*, 239. (c) Tomasi, J.; Persico, M. *Chem. Rev.* **1994**, *94*, 2027. (d) Cossi, M.; Barone, V.; Cammi, R.; Tomasi, J. *Chem. Phys. Lett.* **1996**, *255*, 327.

(17) (a) Gonzalez, C.; Schlegel, H. B. *J. Chem. Phys.* **1989**, *90*, 2154. (b) Gonzalez, C.; Schlegel, H. B. *J. Phys. Chem.* **1990**, *94*, 5523.

(18) Scott, A. P.; Radom, L. *J. Phys. Chem.* **1996**, *100*, 16502.

(19) Andersson, M. P.; Uvdal, P. *J. Phys. Chem. A* **2005**, *109*, 2937.

JP801348W